Supplementary Materials: The Cu(II) – dietary fibre interactions at molecular level unveiled via EPR spectroscopy

Victoria N. Syryamina[a,b], Maxim Yulikov[c] and Laura Nyström[a]

[a] *ETH Zürich, Institute of Food, Nutrition and Health, Laboratory of Food Biochemistry, Schmelzbergstrasse 9, 8092, Zürich, Switzerland*

[b] *Voevodsky Institute of Chemical Kinetics and Combustion of the Siberian Branch of the Russian Academy of Sciences, 630090, Novosibirsk, Russia*

[c] *ETH Zürich, Department of Chemistry and Applied Biosciences, Laboratory of Physical Chemistry, Vladimir-Prelog-Weg 2, 8093, Zürich, Switzerland*

Contents:

S1. SEC data.

The scaling of the polymer was checked by measuring the molecular weight Mw and hydrodynamical radius (R_h) for the DFs by high-performance size exclusion chromatography (HPSEC) (OMNISEC, Malvern Panalytical Ltd., Malvern, United Kingdom). The system consisted of an OMNISEC RESOLVE chromatography compartment combined with a pump, an autosampler, and a column oven equipped with two A'6000M columns in series (8.0 × 300 mm, Viscotek, parent organization: Malvern Panalytical Ltd., Malvern, United Kingdom). OMNISEC RESOLVE detector compartment was equipped with a low and right-angle laser light scattering detector (LALS/RALS), a refractive index (RI), a UV detector and a viscometer. OMNISEC software version v.10.30 was used for data acquisition and analysis. A MiliQ water was used as mobile phase. The temperature of both columns was kept at 30°C, and the flow rate was 0.7 mL/min with an injection volume of 100 µL. Samples were dissolved in the mobile phase at a concentration of 0.1% (w/v) and filtered through a 0.45-µm nylon filter prior to injection. The polyethyleneoxide (PEO, Mw = 24 kDa) and dextran (Mw = 68kDa) were used for calibration.

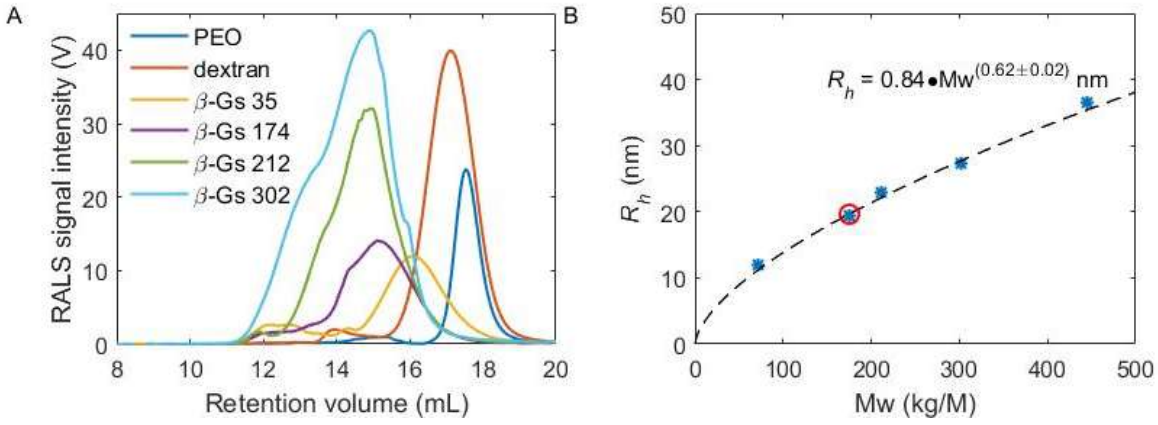

Fig. S1. A. The dependence of the retention volume for different β-glucans (marked as β-Gs Mw in kDa) and the standards – PEO24 and dextran-68. B. The R_h dependence on the polymer molecular weight for barley β-glucans from SEC data. The scaling law is shown by dashed line. The red circle shows the polymer in the work.

S2. Dependence of the longitudinal relaxation time from the transverse-relaxation filtration.

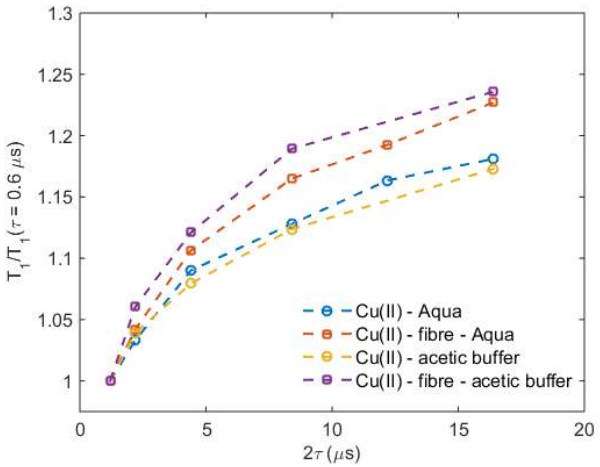

Fig. S2. Dependence of the apparent longitudinal relaxation time T_1 on delay τ varying in the Hahn echo detection sequence, normalized to the T_1 value at τ = 0.6 μs.

S3. Parameters of RIDME traces.

RIDME measurements were aquired at the optimal temperature of 20 K, where the ratio of T_1 and T_m relaxation times for Cu(II) ions in the DF samples is closest to $T_1/T_m \sim 5$.

Table S1. The *d* and *k* parameter of the stretching exponential fit of RIDME traces. If not specified otherwise, the Cu(II) concentration is 312 μM.

Sample composition	d^a			k^b, ms^{-1}		
	τ_2 = 2.2 μs	τ_2 = 4.2 μs	τ_2 = 8.2 μs	τ_2 = 2.2 μs	τ_2 = 4.2 μs	τ_2 = 8.2 μs
Cu(II)-water	4.17	4.23	4.68	246	179	116
Cu(II)-water-fibre	4.02	4.32	5.1	288	208	133
Cu(II)-Acetic buffer	3.45	3.48	3.51	211	165	108
Cu(II)-Acetic buffer-fibre	3.39	3.39	3.39	221	173	114
Cu(II)-Water 1.38 M ^{1}H	3.99	3.99	3.93	213	160	111
Cu(II)-Water 1 mM Cu(II)	3.87	4.35	5.19	324	240	154
Cu(II)-water-fibre 1 mM Cu(II)	3.75	4.14	5.01	329	243	159

[a] the uncertainty in the *d* value determining is about 0.1-0.2;

[b] the uncertainty in the *k* value determining is about 2-5 ms^{-1};

In the aqueous solvent at the same length of the dipolar trace, the dimension parameter in the fibre-containing samples (d = 4.02±0.2) is slightly lower than without fibre (d = 4.17±0.2) and it increases with increasing τ_2 value. A similar behavior is seen in the acetic buffer, but the difference in the d values does not exceed 3%. As the d value affects the decay constant rate, to eliminate the effect of different dimensions, the k value was calculated also with another dimension parameter: in the fibre-free composition the d was set the same as in the composition with DF particles and the corresponding k value was determined and *vice versa*.

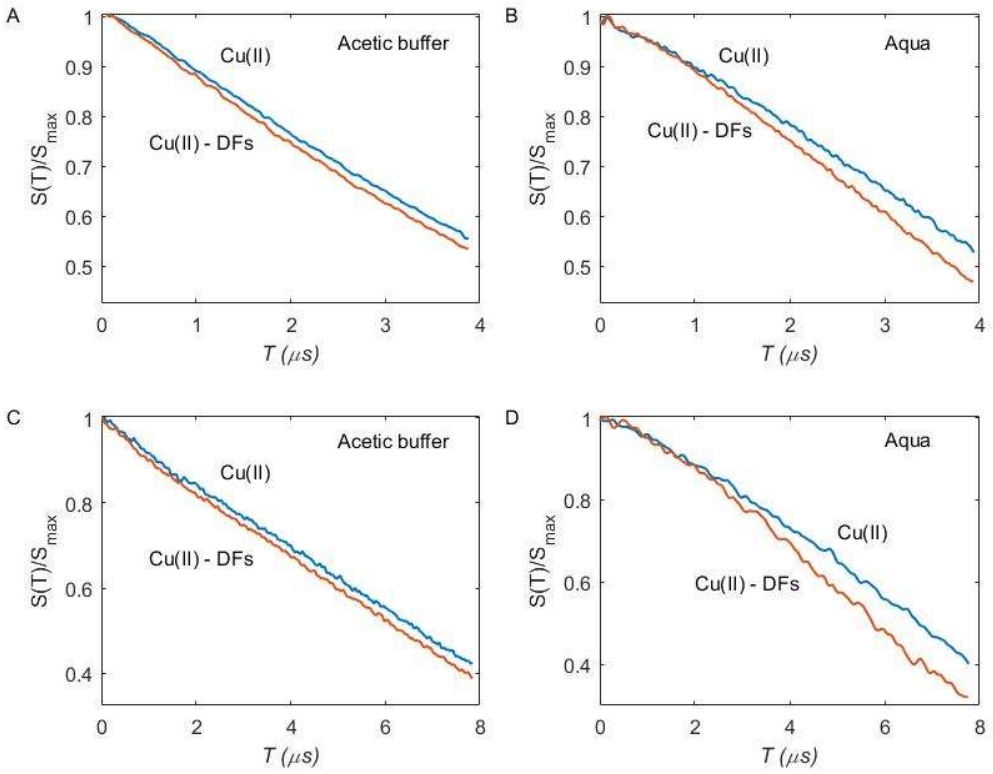

Fig. S3. RIDME traces in the acetic buffer (A, C) and aqueous solution (B, D) with (orange) and without (blue) DF particles at dipolar evolution times of 4 and 8 μs.

S4. The impact of τ_2-filtration effect in DEER and RIDME measurements.

Due to significant g-anisotropy of Cu(II) EPR signal, which causes increasing spectral width with increasing strength of the applied static magnetic field, DEER measurements at lower frequency (X-band) are not necessarily less sensitive that at higher frequency (Q-band). A temperature of 10 K was chosen for DEER experiments, as the low-temperature limit of T_2 is attained at 10 K and T_1 = 900 µs is sufficiently long to avoid substantial longitudinal relaxation during the required total sequence length of 10 to 40 µs.

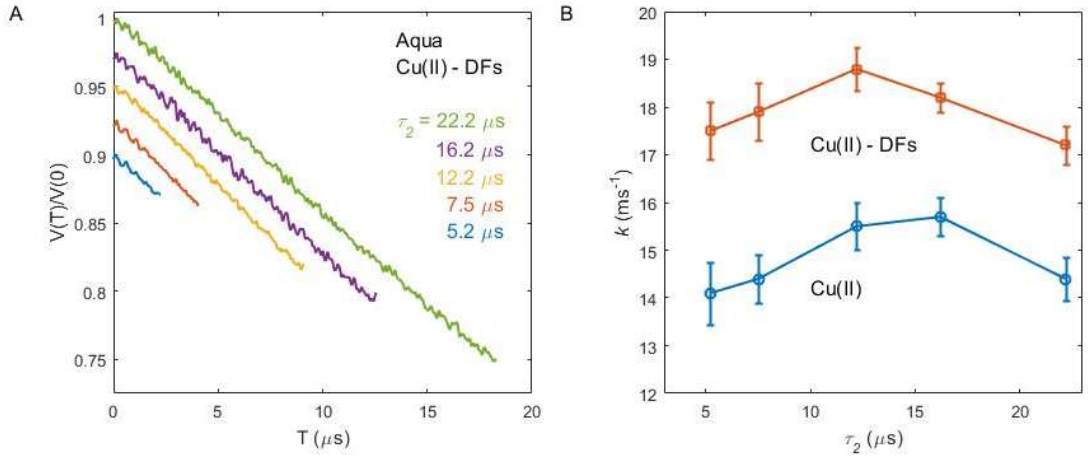

Fig. S4. A) DEER traces in aqueous solution with fibre at different values of the τ_2 time delay. B) The DEER decay rate constant for Cu(II) with (orange) and without (blue) DF particles in aqueous solvent.

The τ_2-filtration effect at short dipolar evolution times is underestimated due to non-suppressed ^{2}H ESEEM. At longer evolution time the filtration effect results in a decreasing the decay rate.

For the case of aqueous solvent, the modulation depth for DEER was estimated above to be p_B=0.049, and this value is only due to the electron dipolar couplings. For RIDME at T_{mix}=1.3·T_1 the upper estimate of the dipolar modulation depth is p_{RIDME}=(1-exp(-T_{mix}/T_1))/2 = 0.36. (1) Combining the latter value with the spin density estimated from the DEER data, we find that the RIDME decay rate at short τ_2 duration exceeds the expected value ca. 2.25 times, which implies the presence of an additional echo decay mechanism in the RIDME experiment. The increase of the τ_2 delay results in decreasing the decay rate in the DEER experiment (Fig. S3), but does not change significantly the contrast between fibre-free and fibre-containing samples, while in the RIDME experiment increase of the dipolar evolution time decreases the contrast in both solvents; which means the presence of an additional

nuclear-spectral-diffusion-based or *relaxation-filtration-based* mechanism which contributes to the RIDME decay rate. (2)

The first mechanism is due to irreversible dephasing of the electron coherence coupled to a nuclear subsystem, since nuclear flip-flops can also occur during the transverse evolution of electron spin coherence. Such nuclear flip-flops result in additional dephasing of the "observation" spins and decrease the intensity of the RIDME echo with increasing delay of the mixing block from the time point where all observer spins are refocused. Besides that, both T_1 and T_m relaxation times for Cu(II) species in the DF sample are broadly distributed, since a stretched exponential decay arises from a continuous distribution of mono-exponential decays with varying relaxation time. Thus, both DEER and RIDME decays at longer τ_2 values have enhanced contributions from species with longer relaxation times. However, the RIDME experiment is intrinsically more sensitive to spectral diffusion than DEER, and thus RIDME is more affected by different filtration mechanisms. Note that both described filters have an increasing impact with increasing τ_2, and might have different impact for fibre-free and fibre-containing compositions.

S5. Estimation of DF particles capacity to the Cu(II) absorption by retention experiments.

If metal ions are preferentially absorbed by DFs, their concentration increases inside DF particles and decreases in the bulk solution outside. We did not detect a difference in the shape of CW EPR spectra in the presence and absence of DFs at room temperature due to fast tumbling. Thus, we performed an experiment, where a small aliquot of the solution volume was taken, the DF particles were removed by filtration, and the Cu(II) concentration was measured by CW EPR. The same CW EPR measurement was performed for a sample without DFs. Filtration of the sample with DF particles was achieved by soft centrifugation using filters with a molecular weight cutoff of 35-60 times smaller the molecular weight of the individual fibre molecule. Typically, the aliquot volume did not exceed 10% from the initial sample volume.

In the CW EPR measurements, the uncertainty for the sample length varies between 2-4 mm and the inhomogeneity of the B_1 field over the sample for the Bruker Super High Q probehead resonator has been taken into account. (3) To provide an accurate reference, the blank solution without DFs was also filtered through the same type of membrane under the same rotation speed. Note that in this experiment the impact of the filtration membrane was crucial – for both the blank sample and sample with the DFs the portion of bound Cu(II) species by the membrane depended on the filtration cycle and had a saturation-like behavior, as it is shown in Fig. S5. The dependence, which may arise from absorption to the filter membrane, was fitted within the Langmuir adsorption model and considered as a background signal. The difference between the fibre-containing samples and the background signal was almost independent on the membrane saturation cycle and characterizes the fraction of the retained copper ions, as it is shown in Fig. S6 for $CuSO_4$ in the aqueous solvent and $Cu(OAc)_2$ in the acetic buffer. However, at filtration with DF particles, above a certain amount of the filtrate passed though the membrane a negative value were observed, which can be caused by membrane blockage by DF particles. Thus, the retention experiments with dietary fibres give only a rough estimate of the fraction of retained ions, which is at the same value in the acetic buffer and the aqueous solvent and accounts for ca. 3 metal ions per one DF particle (absorption capacity is 16.8 μmol/g).

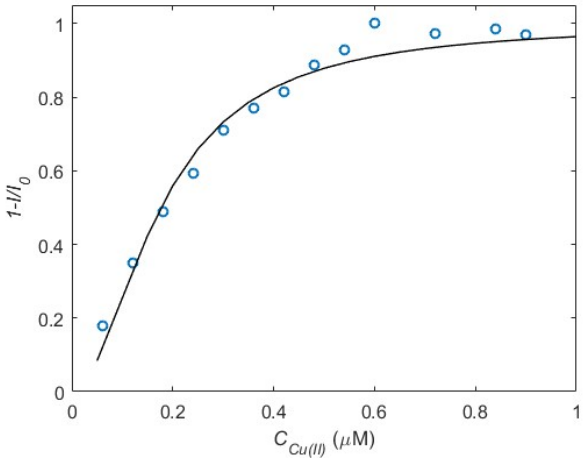

Fig. S5. The example of the PES membrane saturation by Cu(II). The $C_{Cu(II)}$ is an amount of Cu(II) species filtered through the membrane, I and I_0 are the CW EPR signal intensity Cu(II) ions in the filtrate and before filtration, respectively. Circles are experimental results, solid line is a best fit by the Hill equation.

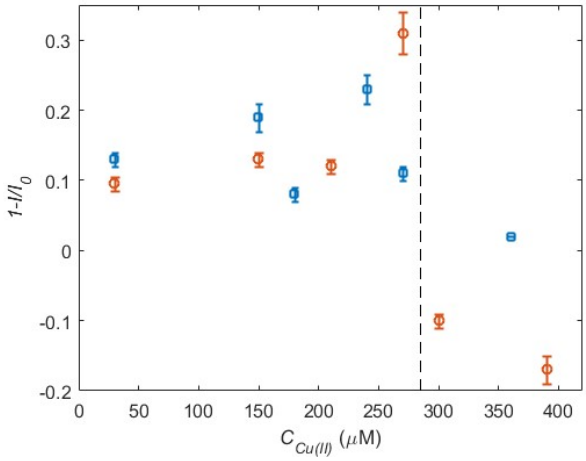

Fig. S6. Results of retention experiments with DF particles. Circles – $Cu(OAc)_2$ in the acetic buffer, squares - $CuSO_4$ in the aqueous solvent. The vertical dashed line shows the approximate value of the filtration cycle above which the PES membrane was blocked.

S6. The mathematical convergence of Monte Carlo simulation.

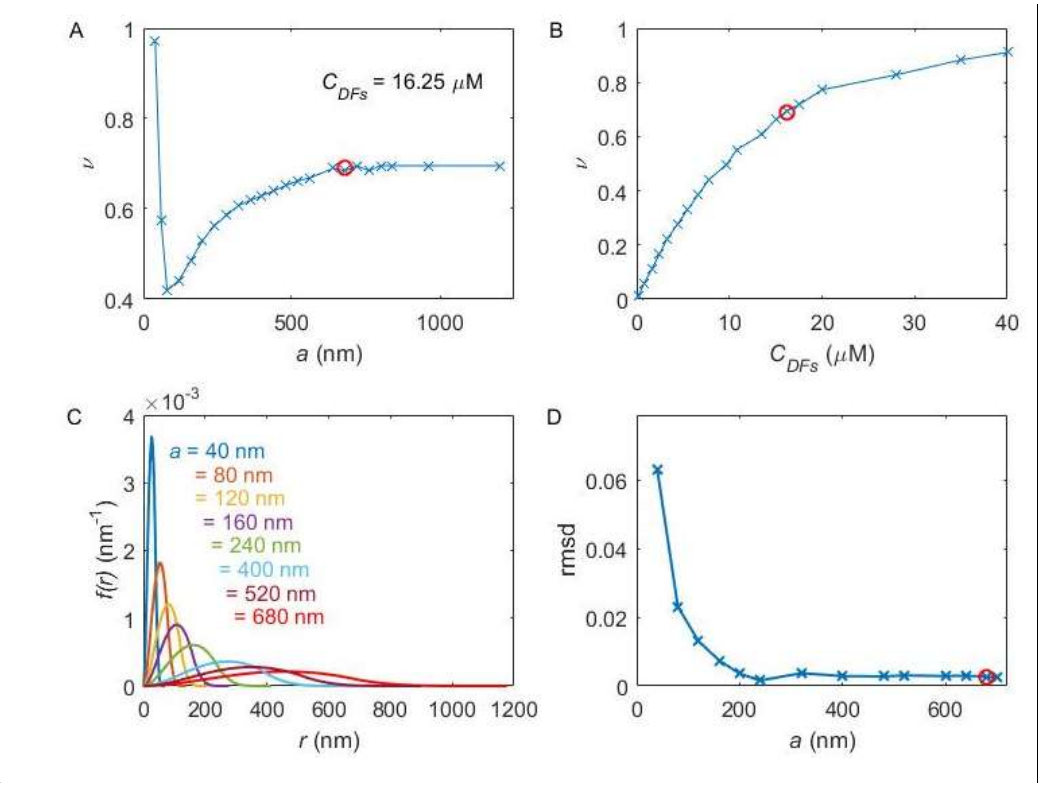

Fig. S7. Demonstration of the convergence of simulation of spin distribution in the space (box with size *a*) for a spins concentration of 312 μM and concentration of DF particles of 16.25 μM. A) The convergence of the filling factor of DF particles at varying box size *a*. B) Filling factor ν at different concentration of DF particles. C) The probability to find the spin partner at the distance *r (f(r)* function) for uniform distribution in the space at varying the box size *a*. D) The difference between theoretical and simulated dipolar decay by using *f(r)* in panel C) as a function of box size *a*. Red circles demonstrates parameters used for a simulation results in Fig. 7A-F.

Computation costs are determined by two factors: the spin concentration and the box size. Increasing the first one requires increasing the second one, which results in abrupt growing of the computation time. The convergence for a system under study is limited by size of individual DF particles. Since the filling factor at 16.25 μM concentration of DFs converges at *a* = 800 nm, we used this box size. Available computation time limited the simulation of larger filling factors at a given radius of DF particles, which constrained the simulations shown in Fig.7A-F.

S7. A note on the HFS analysis of coordination sphere.

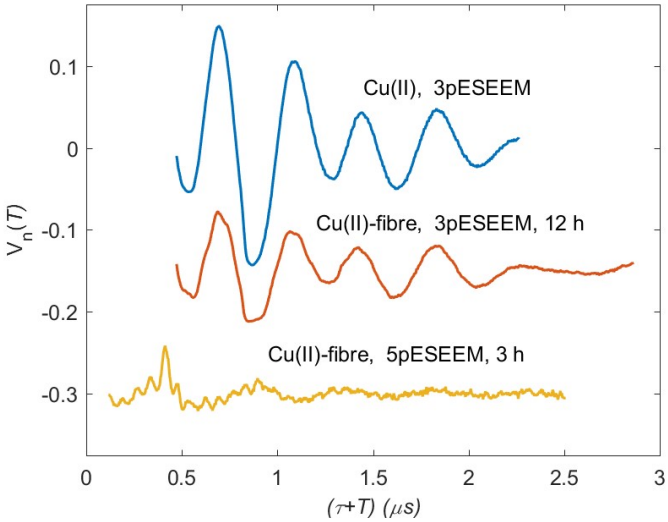

Fig. S8. The 3- and 5-pulse normalized ESEEM traces for Cu(II) with and without fibre in the aqueous solvent. The spike at (τ+T) = 0.412 μs is a not completely suppressed echo crossing effect.

The ^{1}H signal is hardly seen in the 3-pulse ESEEM experiment for Cu(II) in the deuterated aqueous solvent with and without DFs. The 5-pulse ESEEM experiment (4) enhances the ^{1}H signal and requires less measuring time, but the resolution is still not enough for evaluation the hyperfine coupling between Cu(II) species and ^{1}H nuclei. Thus, the ^{1}H ENDOR spectroscopy is more suitable for evaluation the Cu(II) coordination by DFs.

We also checked for presence of a ^{31}P ENDOR signal to exclude Cu(II) binding by phytic acid, which is usually found in cereal fibres as a contamination. The commercial fibre contains traces of phytic acids - for a 17.95 mM β-glucan monomers concentration the concentration of phytic acid is approximately 1.25 μM, (5) which can bind less than 0.5 % of all Cu(II) ions in the sample. The model compound - $CuSO_4$ with an excess of phytic acid in aqueous solution indeed shows a ^{31}P signal, which was however not detected in fibre-containing samples.

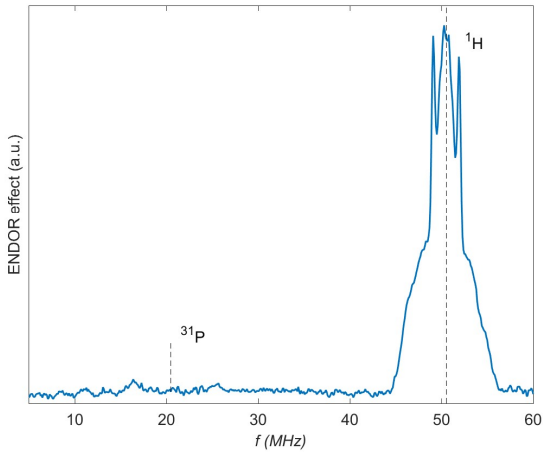

Fig. S9. Davies ENDOR for $CuSO_4$ in the aqueous solvent with an excess of the phytic acid. Vertical dashed lines show the ^{31}P and ^{1}H Larmor frequencies.

References.

1. *Improving the accuracy of Cu(II)–nitroxide RIDME in the presence of orientation correlation in water-soluble Cu(II)–nitroxide rulers.* ***Ritsch, I.; Hintz, H.; Jeschke, G.; Godt, A.; Yulikov, M.*** *Phys. Chem. Chem. Phys., 2019, 21(19), 9810-983.*
2. *Mapping the Structure of Metalloproteins with RIDME.* ***Astashkin, A. V.*** *Methods in enzymology, 2015, 563, 251-284.*
3. *Improving B1 field homogeneity in dielectric tube resonators for EPR spectroscopy via controlled shaping of the dielectric insert.* ***Syryamina, V. N.; Matveeva, A. G.; Vasiliev, Y. V.; Savitsky, A.; Grishin, Y. A.*** *J. Magn. Reson., 2020, 311, 106685*
4. *Electron-spin-echo envelope modulation with improved modulation depth.* ***Gemperle C.; Schweiger A.; Ernst R. R.*** *Chem. Phys. Lett., 1991, 178(5-6), 565-572.*
5. ***Boulos, S.*** *Mass Spectrometric and Kinetic Investigation of Cereal β-Glucan Oxidation (Doctoral dissertation, ETH Zurich). 2016.*